RESEARCH ARTICLE

Processing map to control the erosion of Y_2O_3 in fluorine based etching plasmas

Moritz Kindelmann[1,2] | **Moritz L(ukas) Weber**[1,2,3,4] | **Mark Stamminger**[5] |
Rahel Buschhaus[5] | **Uwe Breuer**[6] | **Martin Bram**[1,7] | **Olivier Guillon**[1,2,8]

[1] Forschungszentrum Jülich GmbH, Institute of Energy and Climate Research 1: Materials Synthesis and Processing, Jülich, Germany

[2] Institute of Mineral Engineering, RWTH Aachen University, Aachen, Germany

[3] Forschungszentrum Jülich GmbH, Peter-Grünberg-Institute 7: Electronic Materials, Jülich, Germany

[4] Jülich Aachen Research Alliance, JARA-FIT, Jülich, Germany

[5] Ruhr University Bochum, Institute for Experimental Physics II, Bochum, Germany

[6] Forschungszentrum Jülich GmbH, Central Division of Analytical Chemistry, Jülich, Germany

[7] Ruhr University Bochum, Institute for Materials, Bochum, Germany

[8] Jülich Aachen Research Alliance, JARA-Energy, Jülich, Germany

Correspondence
Moritz Kindelmann, Forschungszentrum Jülich GmbH, Institute of Energy and Climate Research, 52425, Jülich, Germany.
Email: m.kindelmann@fz-juelich.de

Abstract

Due to the increasing number of applications for ceramic components in reactive etching processes, the interest in the specific erosion behavior of highly etch-resistant materials like yttrium oxide (Y_2O_3) has increased in the past years. Despite the large number of investigations already existing in this field, a more general understanding of the erosion mechanisms still lacks due to the limited comparability of these investigations. The huge difference in the kind of etching setups, processing parameters (bias voltage and plasma gas composition), and sample microstructures prevented consistent conclusions so far. To achieve a more general understanding, this study investigates the erosion behavior Y_2O_3 under a broad spectrum of plasma etching parameters. Therefore, the bias voltage is increased from 50 to 300 V and the plasma gas composition is gradually changed from Ar-rich to CF_4-rich compositions. This systematic approach allows to directly correlate the morphology changes caused by plasma erosion with the related plasma etching parameters and enables to better understand their influence on the depth of physical and chemical interactions, surface damage, and etching rate. We discovered three distinct erosion regimes, which exhibit specific erosion characteristics. Using these observations, a schematic processing map for Y_2O_3 was developed, which could help to estimate the severity of the erosion attack dependent on the processing parameters.

KEYWORDS
erosion mechanism, plasma etching, plasma processing, yttria

1 | INTRODUCTION

In recent years, oxide ceramic materials like yttrium oxide (Y_2O_3) are increasingly applied as consumables in semiconductor etching devices due to their significantly improved erosion resistance in comparison to commercial high purity quartz glass.[1–4] However, the low sinterability of Y_2O_3 powders prevents conventional processing routes like pressing and sintering.[5] As an alternative, various coating technologies were developed to deposit functional Y_2O_3 coatings on quartz glass or Al_2O_3 substrates to increase their erosion resistance.[6,7] Especially aerosol

deposition[1,8] and thermal spray techniques[8–10] are established in the industry for applying Y_2O_3 or other rare earth oxide coatings.

With respect to the literature, the intrinsic erosion of polycrystalline Y_2O_3 under reactive plasma etching conditions is a physicochemical process. On the one hand, there is a chemical degradation of the surface, which is driven by the reactive plasma species (in most cases carbofluorides such as CF_4, C_2F_4, and C_4F_8). On the other hand, physical removal of the reaction products by ion sputtering takes place.[11,12] The formation of nonvolatile reaction products during plasma exposure results in much lower etching rates as compared to SiO_2 based components, which form gaseous reaction products.[13,14] A first general description of the erosion mechanism of Y_2O_3 was reported by Miwa et al. separating the erosion in three stages: fluorocarbon deposition, chemical interaction between fluorocarbons and Y_2O_3, and material removal by physical sputtering.[2] However, in conventionally processed Y_2O_3 ceramics material removal takes predominantly place at residual porosity, which leads to the formation of a crater-like surface.[15,16]

Therefore, the field-assisted sintering technology/spark plasma sintering (FAST/SPS) has been introduced as a single-step consolidation process enabling high-quality components for plasma etching devices yielding materials with a minimal degree of residual porosity.[17–19] This helps to reduce porosity-induced plasma erosion—usually the dominating erosion mechanism—to a minimum.[15,16] Nearly pore-free samples are a prerequisite for studying the intrinsic erosion mechanisms of polycrystalline Y_2O_3.[20,21]

Our recent studies applied this procedure to obtain novel insights into the erosion mechanisms of Y_2O_3. The gathered results clearly reveal that in the case of polycrystalline Y_2O_3 the microstructure and crystalline orientation have a significant influence on the erosion.[20,21] Especially the crystallographic orientation of grains at the surface influences the surface topography that appears after plasma exposure. After exposure, a plateau-like topography was observed,[20] which has not been reported in the literature before. However, the occurrence of this specific kind of erosion seems to depend strongly on the etching parameters. Up to now, the literature describes the formation of a crater-like surface[16,22] and a predominant erosion of residual porosity[15] as main structural changes after plasma exposure.

Even if a lot of reports exist that describe the general behavior of Y_2O_3 coatings as well as bulk samples in plasma environments, the large variety of experimental setups and applied etching parameters impedes an objective comparison between the results and, therefore, prevents more general conclusions at the present state. Little attention has been paid so far on the formation of a grain orientation-related surface topography after plasma exposure, even though this is expected to be critical with respect to the formation of versatile abrasive particles.[10] Particle formation can be a critical issue in plasma etching devices leading to a detrimental damage of the processed wafer. This effect is usually caused by materials, forming solid reaction products during plasma exposure.

In order to make well-founded statements about the specific risks of plasma exposure for Y_2O_3, the erosion behavior of dense polycrystalline Y_2O_3 samples was investigated by systematically varying the plasma etching parameters, in our case the applied bias voltage and the plasma gas composition. By doing so, we were able to distinguish between three distinct regimes of erosion effects, which depend on the etching parameters and strongly influence the etching rate as well as the surface damage during plasma exposure. Based on these experimental results, we were able to derive a schematic processing map, which characterizes the erosion response depending on the plasma processing parameters.

2 | EXPERIMENTAL SECTION

In this study, commercial, highly pure Y_2O_3 powder (99.99 % purity; KDL Resources, USA) was used as the starting material. The content of elemental impurities was determined by inductively coupled plasma (ICP) mass spectroscopy (ICP-MS; Agilent 7900, USA). The detected impurities were traces of 4 ppm Si, 20.0 ppm Ca, 1.9 ppm Zn, 0.2 ppm Sr, 0.6 ppm Ba, and 0.1 ppm Ce at a very low level. Important for the desired application, the powder did not contain Co, Na, Ni, and Ti impurities, which are critical elements in the processing chain of semiconductors. In the as-delivered state, the powder was strongly agglomerated with a median agglomerate size of 5.2 ± 0.1 μm (determined by laser granulometry; LA-950 HORIBA Scientific, Japan). The primary crystallite size was 60 ± 17 nm (determined by TEM). Without further treatment, the powder was less suitable for conventional processing by pressing and sintering. Therefore, field-assisted sintering technology–spark plasma sintering (FAST–SPS) was used to produce polycrystalline Y_2O_3 specimens with a high relative density (above 99%) in a single sintering step. High densities are crucial to avoid that material removal starting from the edge of residual pores dominates the erosion process,[15,16] superimposing the intrinsic erosion behavior of the respective material itself. FAST–SPS was done in an HP-D5 device (FCT Systeme, Germany). All samples were processed in cylindrical graphite tools with a diameter of 12 mm and the sintering temperature, heating rate, uniaxial pressure, and dwell time were fixed at 1500°C, 100°C/min, 50 MPa, and 10 min.

TABLE 1 Plasma etching parameters applied in this study to investigate the influence of bias voltage (B) and the influence of plasma gas composition (C) on the erosion behavior

Sample	U_b [V]	Ar [sccm]	O_2 [sccm]	CF_4 [sccm]	CF_4 [%]
B50	50	5.0	0.3	1.0	20
B150	150	5.0	0.3	1.0	20
B300	300	5.0	0.3	1.0	20
C5	150	9.5	0	0.5	5
C10	150	9.0	0	1.0	10
C40	150	6.0	0	4.0	40
C80	150	2.0	0	8.0	80

To obtain samples free of graphite impurities and chemically reduced surfaces, graphite foil residues were removed by mechanical grinding followed by a postthermal treatment at 1200°C for 4 h in air to regain oxygen stoichiometry. Before exposing the samples to the plasma atmosphere, ceramographic preparation was used to reduce the thickness of samples below 1 mm and gain a mirror-polished surface finish. The final polishing step was performed with a 1 μm diamond suspension, yielding a well-defined, mirror-like surface to exclude that surface roughness and other preparation-related surface features like scratches influence the erosion process.

The plasma experiments conducted in this study were performed in a laboratory-scale ICP reactor using an Ar, CF_4, and O_2 mixture as plasma gas. Details on the experimental setup can be found elsewhere.[20] During all plasma experiments, the working pressure and the ICP power were kept constant at 0.02 mbar and 600 W, respectively. Further, the exposure time was fixed at 120 min to ensure a good comparability between experiments under varied bias voltage and different compositions. To gain more knowledge about the influence of varied bias voltages and gas composition, both parameters were systematically changed, and the associated erosion response was investigated thoroughly. Therefore, the bias voltage was changed between 50, 150, and 300 V at a fixed plasma gas composition of Ar (5.0 sccm), CF_4 (1.0 sccm), and O_2 (0.3 sccm) corresponding to a CF_4 volume percentage of 20% (oxygen excluded). In a second set of experiments, the plasma gas composition was varied from an Ar-rich composition (Ar [5.7 sccm], CF_4 [0.3 sccm]) to a CF_4-rich composition (Ar (1.2 sccm), CF_4 [4.8 sccm]) at a constant bias voltage of 150 V. All investigated processing parameters are summarized in Table 1.

After the plasma exposure, the surface topography and the reaction layer formed on the sample surface were investigated using different characterization methods. The surface topography was determined by atomic force microscopy (AFM; Cypher, Oxford Instruments Asylum Research Inc; USA). Measurements were done in the tapping mode and analyzed using the software package Gwyddion. The derived topographic data were postprocessed by using the align rows as well as the remove background function to allow a reproducible comparison of different AFM scans. Additionally, scanning electron microscopy (SEM, Zeiss Cross Beam XB540, Germany) was used to characterize the surface topography and validate the AFM results.

For a deeper understanding of the reaction layer formed after plasma exposure, transmission electron microscopy (TEM; Tecnai F20; FEI, USA) was applied in high resolution (HR TEM) mode. This allows to conclude on the depth of physical interaction induced by the plasma exposure. A focused ion beam (FIB; FEI STRATA FIB 205, USA) was applied to extract lamellae from a representative area of the surface. Additionally, the chemical composition at the surface was investigated by time-of-flight secondary ion mass spectroscopy (TOF-SIMS; ION-TOF, Germany). This is especially important to understand how the change of plasma gas composition from Ar-rich to CF_4-rich compositions influences the chemical degradation of the surface. Therefore, intensity profiles of F^-, O^-, C^-, and Y^- ions were measured allowing a direct comparison of the interaction depth. The applied TOF-SIMS device used Cs^+ ions (1 keV, 57 nA) to remove material from the surface forming a 300 × 300 μm sputter crater. Bi^{3+} ions (30 keV, 26 pA) were used for elemental analysis in the center of this crater. Finally, the etching rate was determined for samples subjected to different plasma compositions. Here, parts of the Y_2O_3 surface were covered by a plasma resistant polyimide tape, and the height of the etching step formed at the edge of the tape after a distinct exposure time was analyzed to conclude on the etching rate. As a reference, in all experimental series, pure silica glass samples (Spectrosil, Heraeus Quarzglas GmbH, Germany) were positioned in the plasma chamber to compare the performance of FAST/SPS processed Y_2O_3 to commercially available high-quality quartz glass. Depending on the material, AFM or confocal laser microscopy (VK-9710 K,

Keyence, Japan) were applied to determine the etching depth.

3 | RESULTS AND DISCUSSION

In the following, the results of both experimental series are shown in separate sections. For comprehensively discussing the influence of the applied bias voltage, parts of the experimental results from our former studies were considered here.[20,21] To get a more general understanding of the specific erosion mechanisms of polycrystalline Y_2O_3, further targeted experiments at 50 and 300 V were conducted in the present study. To the best of our knowledge, a detailed investigation of how the plasma gas composition influences the erosion of Y_2O_3 is not available in the literature so far.

3.1 | Influence of applied bias voltage

The applied bias voltage is the main driving force for material degradation in reactive plasma etching of polycrystalline ceramics. It is directly coupled with the formation of nonvolatile phases as a result of the chemical reaction with the fluorine-containing plasma species [2,6,16]. This makes the applied bias voltage one of the significant processing parameters due to defining the etching rate, gener-

ated surface topography as well as the physical and chemical interaction in the near-surface area.

In this study, the erosion mechanisms are analyzed by the characterization of the surface topography as well as the reaction layer formation at varied bias voltages and different Ar/CF_4 ratios. Finally, it led to a more general understanding of the material response induced by reactive plasma exposure. An important aspect of our study with respect to the literature is that the application of FAST–SPS allowed us to almost completely exclude the influence of residual pores on the erosion behavior. Therefore, we were able to gain a deeper insight into the intrinsic erosion behavior of polycrystalline Y_2O_3, which is only marginally discussed in the literature so far.

3.1.1 | Surface topography and morphology

Figure 1 shows representative secondary electron SEM images of the surface morphology as a function of the applied bias voltage indicating the strong impact of bias voltage on the topography formation after plasma exposure. In the case of a bias voltage of 50 V (Figure 1A) the surface shows only slight microstructural changes. Grain boundaries and pores tend to be attacked preferentially. At low bias voltage, surface grooving and edge rounding of residual pores were less pronounced, but first changes in the surface morphology when comparing different grains
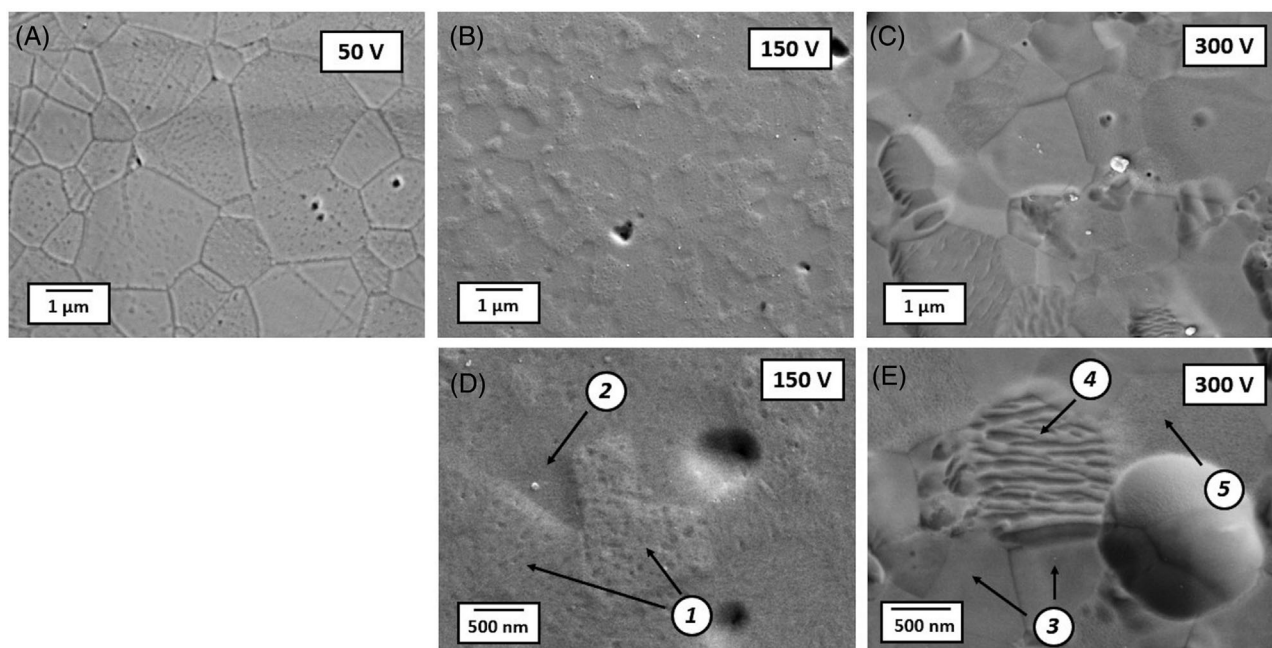

FIGURE 1 SEM images of the surface morphology after a plasma exposure for 2 h under a bias voltage of (A) 50 V (B) 150 V (C) 300V. (D) Detail of a sample exposed to 150 V (E) Detail of a sample exposed to 300 V. Highlighted areas show (1) porous grains, (2) flat grains, (3) flat grains, (4) surface rumpling, and (5) rough grains
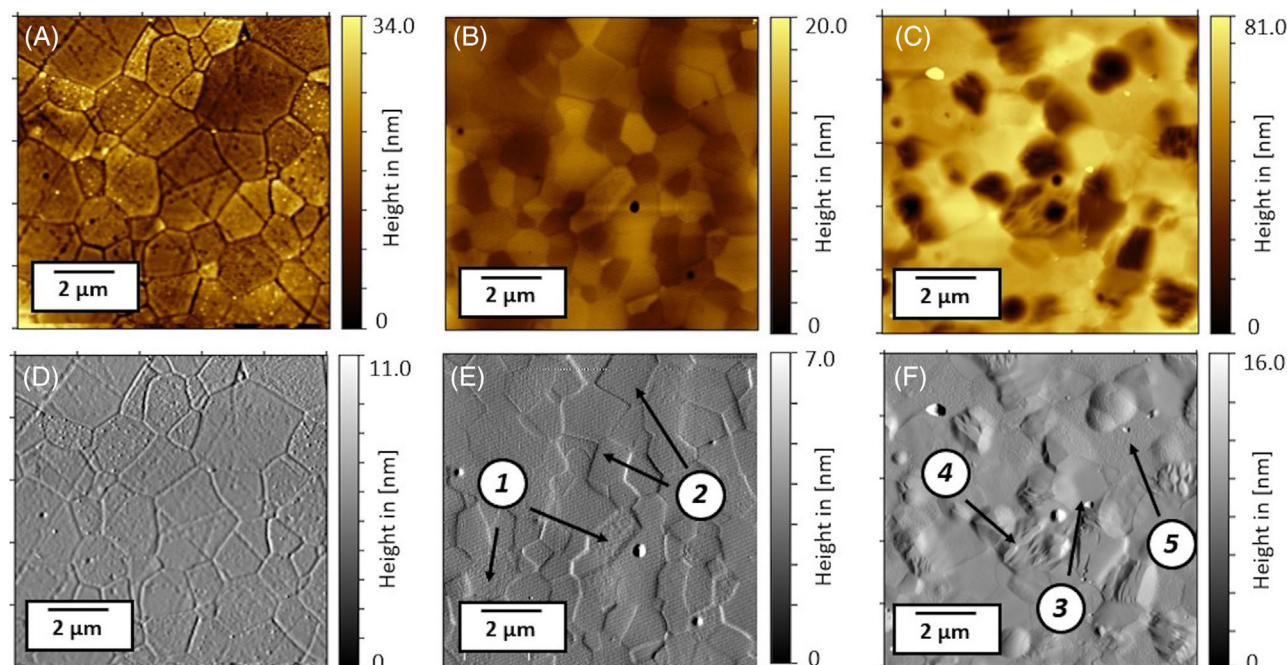
FIGURE 2 Atomic force microscopy (AFM) scans of the surface morphology in topographic and amplitude mode after a plasma exposure for 2 h under a bias voltage of (A,D) 50 V. (B,E) 150 V. (C,F) 300V. Highlighted areas show (1) porous grains after an exposure to 150 V, (2) flat grains after an exposure to 150 V, (3) flat grains after an exposure to 300 V, (4) Surface rumpling, and (5) rough grains

were already visible. Increasing the applied bias voltage to 150 V already strongly changes the surface topography. Part of the grains had a nano-porous appearance after the treatment (Figure 1D, marker 1), while in the case of other grains a flattened surface remained (Figure 1D, marker 2).

Furthermore, a plateau-like surface topography appeared, which depicts the grain structure of polycrystalline Y_2O_3. The specific formation of a microstructure-dependent erosion topography at a bias voltage of 150 V in an Ar-rich plasma gas has been extensively investigated and discussed in our recent studies[20,21] In these connected publications, which investigate the erosion mechanisms and the formation of an reaction layer in-depth two major reasons were identified to be the main reason for the formation of a plateau-like topography: (I) On the one hand, we found a grain orientation dependent material removal, which was induced by an ion transparency effect.[20,23] (II) On the other hand, an orientation-dependent adsorption behavior of the reactive plasma species on the sample surface led to the formation of a reaction layer, dominated by the fluorination of Y_2O_3.[21] The direct correlation of crystallographic orientation and surface topography formation is additionally highlighted in Figure S2. In addition to topographic effects, the small amount of residual pores on the surface shows the rounding of pore edges as well-known from literature.[15,16]

A further increase of the bias voltage to 300 V led to a much more pronounced change of surface topography compared to the microstructure at lower accelerating voltages. The porous surface layer visible in Figure 1B cannot be observed anymore, indicating higher removal rates of the reaction layers formed at the surface Additionally, it is possible to distinguish between three different kinds of microstructure dependent morphologies: smooth and flat surfaces (Figure 1E, marker 3), microstructural rumpling (Figure 1E, marker 4), and rough and flat surfaces (Figure 1E, marker 5). The microstructure-dependent formation of different morphologies hints on removal processes, which depend on the crystallographic orientation of certain grains also at a high bias voltage of 300 V. This behavior did not become obvious from our former works.[20,21] However, STEM-EDX investigations could already highlight the different reaction layer formation under varied bias voltages (Figure S2).

Further investigations of the surface topography under different bias voltages were performed by AFM (Figure 2). The topographic scans in Figure 2A,C,E confirmed the increase of surface damage when bias voltages exceeded 50 V. While the topography after the exposure at 50 V left the microstructure almost physically undamaged, bias voltages of 150 and 300 V caused strong topographic changes, which obviously depend on the grain orientation. Furthermore, the amplitude scans displayed in Figure 2B,D,F clearly indicate the formation of different morphologies at low and high bias voltages. The formation of nano-pores inside selected grains was limited
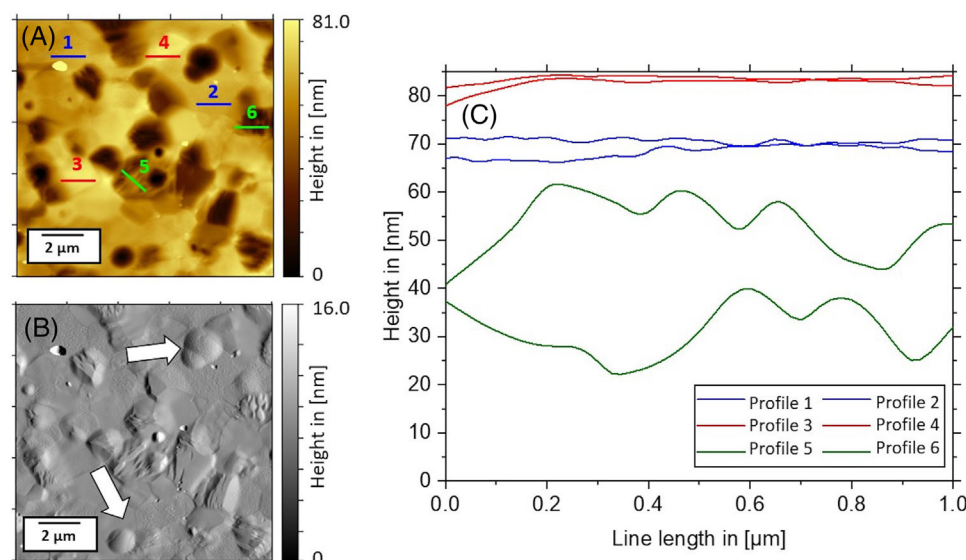
FIGURE 3 Detailed atomic force microscopy (AFM) analysis of the surface morphology after a plasma exposure for 2 h at a bias voltage of 300 V in topographic (a) and amplitude mode (b). Colored lines in (a) mark the position of the AFM line profiles. Arrows in (B) highlight the position of microstructure independent sputtering craters. (C) AFM line profiles extracted from the topography scan indicate microstructure dependent surface morphologies

to intermediate bias voltages while high voltages of 300 V caused a complete removal of material near to the surface.

In addition to the microstructure-dependent topography, high bias voltages suggest an independent, superimposed removal mechanism leading to sputtering craters randomly distributed on the surface. Figure 3 shows details of the AFM scan of a sample surface after being exposed to a bias voltage of 300 V focusing on the microstructure-dependent topography. Line profiles are extracted from the topography scan to highlight different surface morphologies, which were dependent on the underlying microstructure.

Grains represented by red and blue lines exhibited a flat surface and differed only by a slightly increased roughness of certain grains. In contrast, grains indexed by green lines display a clearly rugged surface. This specific morphological effect was observable only at high Ar+ ion energies and indicated a strong orientation dependency, which has been only described so far for metals exposed to plasma environments.[24,25] Furthermore, microstructure independent craters are visible (white arrows), which indicated an additional erosion mechanism superimposing the already described orientation-dependent removal mechanism at high bias voltages. This behavior has been described in several studies investigating the erosion behavior at increased bias voltages.[16,22]

When looking at surface morphologies of polycrystalline Y_2O_3 after plasma treatment at 50, 150, and 300 V, the main observations can be summarized as follows. The variation of the bias voltage led to major differences between the active erosion mechanisms:

1) At 50 V, erosion was almost negligible. Plasma–material interaction is dominated by surface fluorination,[2,11,26] which mainly leads to nonvolatile reaction products. The appearing reaction layer is stable against low-energy sputtering. Therefore, it strongly decelerates the material removal and causes a high resistance against the plasma exposure.

2) Increasing the voltage to 150 V changes the surface reaction and material removal mechanism to a mixed chemical and physical erosion. The deposition of fluorine-containing species on the surface and the related fluorination of Y_2O_3 are in equilibrium with the physically induced material removal through sputtering. This mixed erosion process leads to the observed formation of nano-pores in selected grains indicating the formation of a fluorine reaction layer as well as a microstructure dependent plateau-like topography. A direct correlation between crystallographic orientation and surface topography is given in Figure S1.

3) A further increase of the bias voltage up to 300 V changes the main erosion mechanism toward a physically dominated process. Additional physical erosion mechanisms are activated leading to a topography, which still depends on the initial grain orientation. In addition, microstructure independent sputtering craters appear indicating the onset of severe plasma–material interactions.
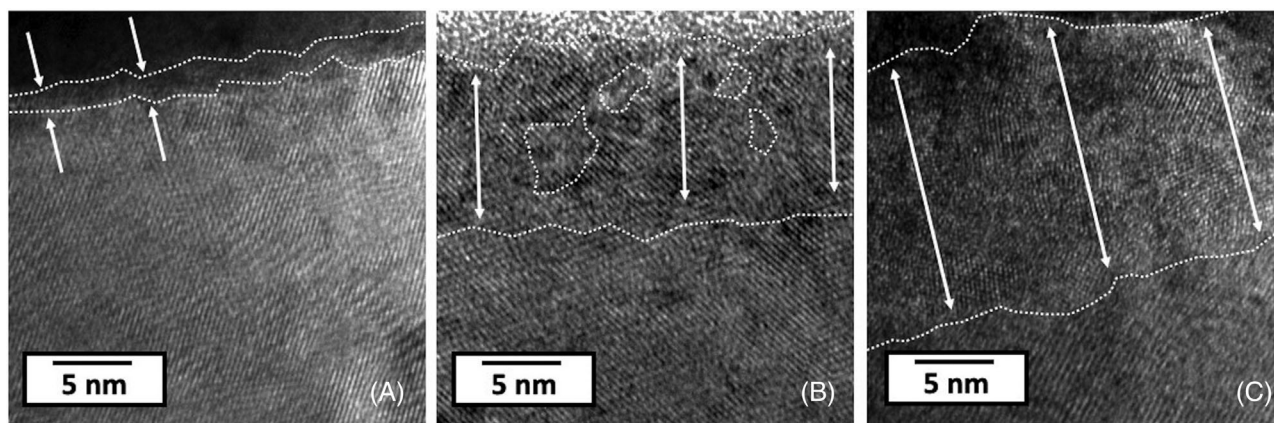
FIGURE 4 HRTEM images of Y_2O_3 after plasma exposure for 2 h under varied bias voltages of 50 V (a), 150 V (b), and 300 V (c). Included arrows illustrate the thickness of the physical interaction layer. Additional marked areas in (b) highlight amorphous regimes, which are embedded in a crystalline lattice

3.1.2 | Reaction layer formation

To get a better understanding of how the physical damage of the sample surface takes place and how deep it impacts the bulk of the samples, FIB lamellae of affected areas were prepared and examined using high resolution transmission electron microscopy (HRTEM). The bias voltage was varied again to 50, 150, and 300 V. Figure 4 shows the cross section of the sample surface at the different bias voltages. With an increasing bias voltage, the depth of the influenced zone on the surface clearly increases. The physical damage at 50 V was almost negligible and is limited only to the surface. Here, only the surface zone is influenced through a reaction with the fluorocarbon deposit. Increasing the bias voltage to 150 and 300 V expanded the affected zone from 10 to 15 nm (Figure 4B,C). This reaction layer consists of a YO_xF_x reaction layer, which shows a chemical gradient from the surface into the bulk (Figure S2). In some areas, there is an indication that amorphous phases have been formed (Figure 4B, marked areas). On the other hand, the crystal structure below the physically affected zone remained unchanged. These results confirm the combined or mixed erosion mechanism that is active during the plasma exposure at high bias voltages. The chemical surface reaction induced by reactive fluorine species is superimposed by physical damage induced by ion irradiation. These results reveal that the physical damage strongly increases with an increase in the incident energy of Ar^+ ions, which is in accordance with literature and the fundamental erosion mechanism first described by Miwa et al. (detailed schematic graph in Figure S3). Large differences in the depth of the affected zone at 150 and 300 V could not be detected, even though different kinds of morphological surface morphologies were observed for these bias voltages by SEM and AFM. This fact makes it obvious that the plasma-induced erosion is an effect, which mainly takes place in a small volume near the surface.

3.2 | Influence of plasma gas composition

In addition to the applied bias voltage, the plasma gas composition also has a significant influence on the erosion behavior of polycrystalline ceramics in the case of plasma exposure. Only a small number of investigations considered this parameter so far. Their focus mainly lied on chlorine-containing etch gases.[9,27,28] The ratio between the chemically reactive plasma species (in this work CF_4) and the ionized plasma component (in most cases Ar) strongly determines the number of reactive atoms and radicals as well as the amount of ionized Ar being the origin of the sputtering effect. The gas composition is expected to change the erosion mechanism from a chemically to a physically controlled mode, having a large impact on the material response like etching rate, particle formation, and resulting surface morphology.

To investigate this in detail, Y_2O_3 samples were subjected to different plasma compositions using a bias voltage of 150 V and an exposure duration of 2 h. The composition (defined by volume percentage of CF_4) was varied from 5%, 10%, 40% to 80% CF_4 (C5, C10, C40, C80; Table 1), leading to corresponding Ar contents 95%, 90%, 60%, and 20%, respectively. The parameters were chosen to cover a broad range from highly Ar-rich to CF_4-rich compositions, allowing conclusions regarding the influence of gas composition on the erosion behavior.
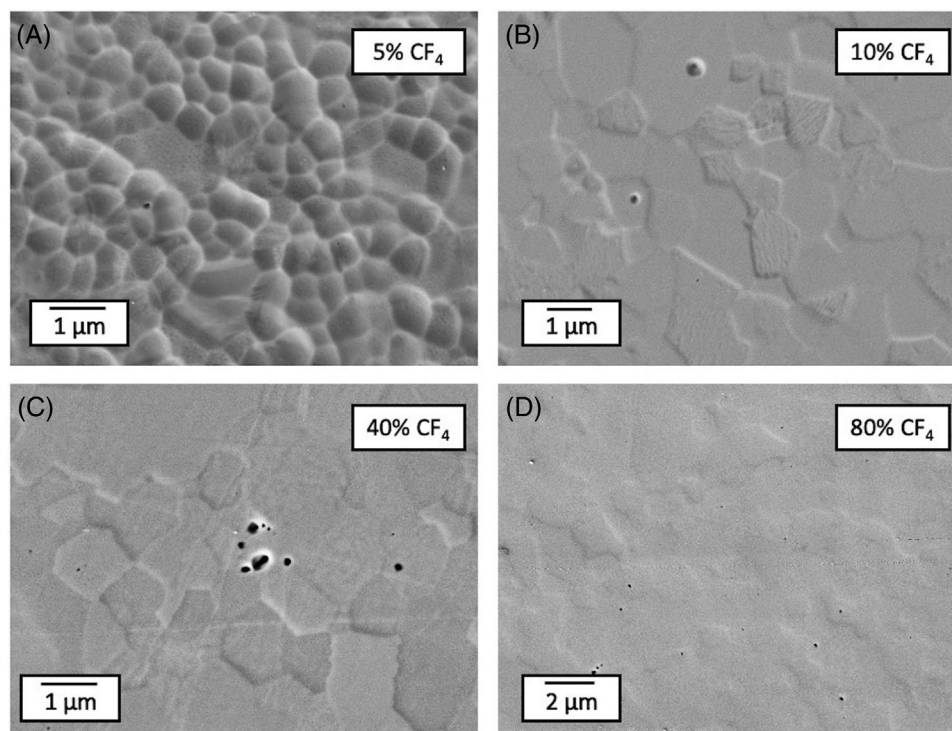
FIGURE 5   SEM images of the surface morphology after a plasma exposure under 150 V for 2 h with a CF_4 volume percentage of (A) 5%, (B) 10%, (C) 40%, and (D) 80%

3.2.1 | Surface topography and morphology

The influence of the CF_4 volume percentage during the plasma exposure on the formed surface topography is characterized by SEM and representative microstructures are displayed in Figure 5. The microstructure at the surface is strongly dependent on the CF_4/Ar ratio and showed three types of erosion modes:

(I) Figure 5A shows a homogeneous distribution of microstructure independent sputtering craters. A comparable surface topography was already observed in samples subjected to high bias voltages (AFM in Figures 2 and 3) indicating a physically dominated etching process.

(II) Figure 5B,C exhibits a microstructure-dependent surface topography, which was already observed at intermediate bias voltages of 150 V with a CF_4 percentage of 20%, indicating a mixed erosion mechanism.

(III) Figure 5D shows a very smooth surface indicating only a minor effect of the initial grain structure.

Comparing the surface topography, using SEM imaging, shed first light on the dominant etching mechanisms in different processing regimes. The characteristic material response of Y_2O_3 depended strongly on the amount of physical and chemical contribution during the exposure. A high proportion of ionized Ar atoms in the plasma or increased bias voltages induced a physically dominated removal process. Material removal by ion sputtering is the rate-controlling mechanism leading to a microstructure independent etch morphology and to high removal rates. During plasma etching, the ongoing fluorocarbon deposition-removal process is shifted strongly toward a fast removal of reactive species from the surface but nevertheless inducing a certain amount of fluorination. Increasing the CF_4 percentage from 5% to 10% and further to 40% shifted the competing degradation processes at the surface more to a mixed chemical-physical regime (M), where a microstructure dependent erosion mechanism became active as indicated by the formation of a surface topography representing the initial grain structure. Hereby, the deposition of the fluorocarbon layer on the surface plays a more dominant role leading to a grain orientation-dependent etching mechanism.[20,21] Replacing large amounts of Ar in the plasma gas composition by CF_4 leads to a chemically dominated erosion (C). Due to the nonvolatile nature of the reaction products that are formed during the chemical plasma attack and the low content of ionized Ar in the plasma chamber, the erosion rate decreased significantly and almost no material removal and erosion damage was observed during SEM investigations.
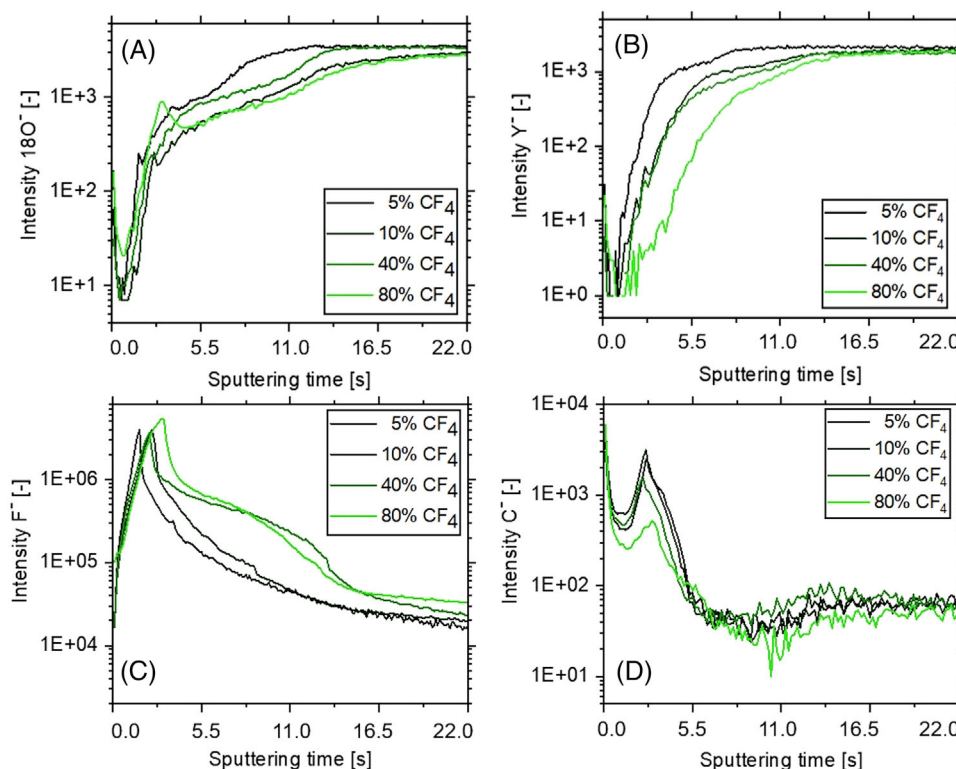
FIGURE 6 Time-of-flight secondary ion mass spectroscopy (TOF-SIMS) depth profiles of all samples tested with different plasma gas compositions. Intensities of relevant elements are visualized in separated graphs showing (A) 18 O− (B) Y− (C) F− and (D) C−ions

3.2.2 | Reaction layer formation and etching rate

For a better understanding of the chemical interaction of the plasma with the bulk material near to the surface, the reaction layer formation at different plasma gas compositions was investigated by TOF-SIMS. Figure 6 shows the chemical gradients of fluorine, oxygen, carbon, and yttrium depending on the sputtering time. The change of the plasma gas composition to higher CF_4 concentrations led to a stepwise change of the chemical gradients at the surface. This observation can be associated with the lower amount of Ar^+ ions in the plasma, which reduces material removal rates and enables an increased fluorine interaction depth, which is especially indicated by the fluorine (Figure 6C) and oxygen (Figure 6B) distributions. The increased CF_4 content causes a higher fluorine penetration and a depletion of oxygen near to the surface in comparison to the profiles related to plasma compositions with a higher Ar/CF_4 ratio. The lower amount of CF_4 in the plasma gas was coupled with a constant and sharp decrease in the fluorine intensity while high CF_4 percentages led to a two-step gradient. The high concentration of Ar^+ ions in the compositions with low CF_4 led to a reaction process dominated by physical sputtering, directly removing fluorine reaction products from the surface and

preventing a more pronounced chemical interaction (physical regime). Similar behavior is indicated by the chemical gradients of oxygen and yttrium. These results confirm the appearance of two clearly distinguishable etching regimes that influence the morphology at the surface after plasma exposure and change the chemical interaction with the bulk material. During a physically dominated erosion, fluorine species are removed quickly from the surface due to high sputtering rates and prevent the formation of a chemical fluorine gradient. Changing the plasma gas composition to the CF_4-rich regime led to an increased fluorine penetration into the bulk, which is coupled with a change of the characteristic run of the gradients (Figure 6C; 40%, 80% CF_4). The chemical gradients of oxygen, yttrium, and carbon behave accordingly, mirroring the gradients introduced by fluorine interaction. This behavior shifts the erosion response to a chemically dominated regime. Here, TOF-SIMS could reveal the stepwise change from physical to chemical-dominated plasma surface interaction, which is induced by the varied plasma gas composition.

Finally, the etching rate is one of the most critical process parameters because it directly influences the lifespan of the sintered component in the plasma etching device. Therefore, the etching rate was determined for polycrystalline Y_2O_3 and amorphous SiO_2 samples at varying gas compositions. The etching rate was calculated from an
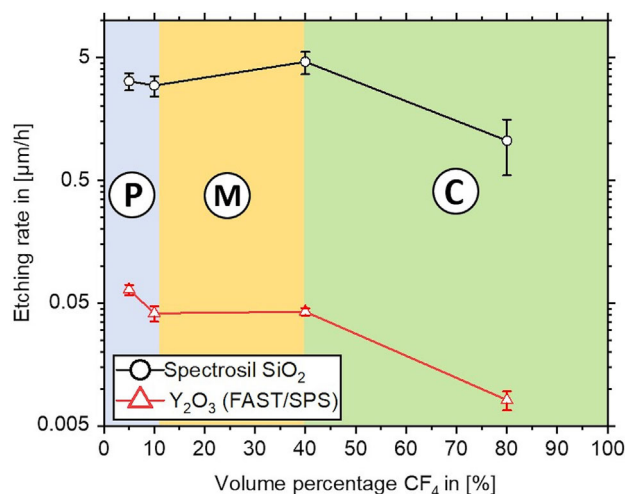
FIGURE 7 Etching rate of Y_2O_3 and SiO_2 depending on the plasma gas composition. The etch rate was determined on an etch step induced through masking parts of the exposed area. All samples were treated with a bias voltage of 150 V and the exposure duration was 2 h. The etch depth was determined using a confocal laser microscope for SiO_2 and an AFM for Y_2O_3. Dominating removal mechanisms are indicated by the background color and abbreviations P, physical; M, mixed; and C, chemical

etch step that formed at the edge of a plasma resistant polyimide mask. The etching rate of both materials as a function of the CF_4 content is displayed in Figure 7. As expected from the results presented before, the plasma gas composition had a strong impact on the etching rate of Y_2O_3 and SiO_2. Ar-rich gas compositions are coupled with the highest removal rates. The comparison of etching rates between Y_2O_3 and SiO_2 clearly demonstrates the significantly improved etching performance of Y_2O_3 ceramics as Indicated by orders of magnitude lower erosion rates. The highest removal rate for Y_2O_3 was observed when physical sputtering was the dominating erosion process. The etching rate slightly decreased in the mixed erosion regime and only very low removal rates were measured when chemical interaction was the dominant mechanism. The specific etching rates confirm the plasma–material interaction behavior as already concluded from the surface morphology investigations. It is possible to derive three distinct regimes, which have a characteristic etching rate, surface morphology, and chemical reaction layer. This is highly dependent on the applied plasma etching parameters bias voltage and plasma gas composition.

A systematic variation of the main processing parameters of plasma etching (bias voltage and plasma gas composition) enabled to draw sound conclusions on the material response of polycrystalline Y_2O_3 with respect to these parameters. As discussed before, the material behavior can be categorized into three different kinds

of characteristic microstructural and chemical types: (P) physically dominated erosion (M) mixed erosion (C) chemically dominated erosion. Based on the main results of the present study and our previous work on the erosion mechanism of yttria in fluorine-based etching plasmas, Figure 8 shows a process parameter–material response map. Visualizing how the bias voltage and gas composition are related to the observed change of the sample surface allows to sketch the active erosion mechanisms in form of a processing map. The observed mixed erosion behavior, which has been discussed in detail already in our recent studies.[20,21] is now completed by a chemically driven erosion regime with minor surface damage and low material removal (C) and a physically driven erosion regime characterized by strong surface damage and high material removal rates (P). This processing map enables to estimate the dominating erosion response at a given parameter set. It is therefore a helpful tool for predicting the lifespan of polycrystalline Y_2O_3 components when exposed to reactive fluorine plasmas. Furthermore, the basic idea behind our processing map can be easily transferred to other ceramic materials to evaluate their erosion behavior under different plasma processing parameters. Therefore, the fundamental approach of our study contributes to a more general understanding of the erosion behavior of ceramic materials under plasma etching conditions.

4 | CONCLUSIONS

In the present work, a systematic variation of the main plasma etching parameters bias voltage and plasma gas composition enabled to draw sound and comprehensive conclusions on the erosion behavior of polycrystalline Y_2O_3. The variation of the bias voltage from 50 to 300 V led to significant changes in the surface morphology. At bias voltages of 150 and 300 V, different microstructure-dependent erosion mechanisms could be observed, which are distinguished by a physicochemical mechanism at 150 V and a pure physical erosion mechanism at 300 V. Vice versa, low bias voltage of 50 V did not reveal strong surface damage due to the low intensity of Ar^+ ion bombardment during exposure. Additionally, TEM investigations highlighted the stepwise increase of the physical interaction depth induced by increasing bias voltages. Furthermore, a stepwise variation of the plasma gas composition from $Ar/CF_4 = 95/5$ to $Ar/CF_4 = 20/80$ clearly revealed three distinct erosion regimes, namely a physically driven, a mixed, and a chemically driven erosion. These erosion regimes are distinguished by their characteristic surface morphology, chemical interaction depth, and etching rate. These findings enabled to derive a schematic erosion regime map. It allows to estimate the active erosion
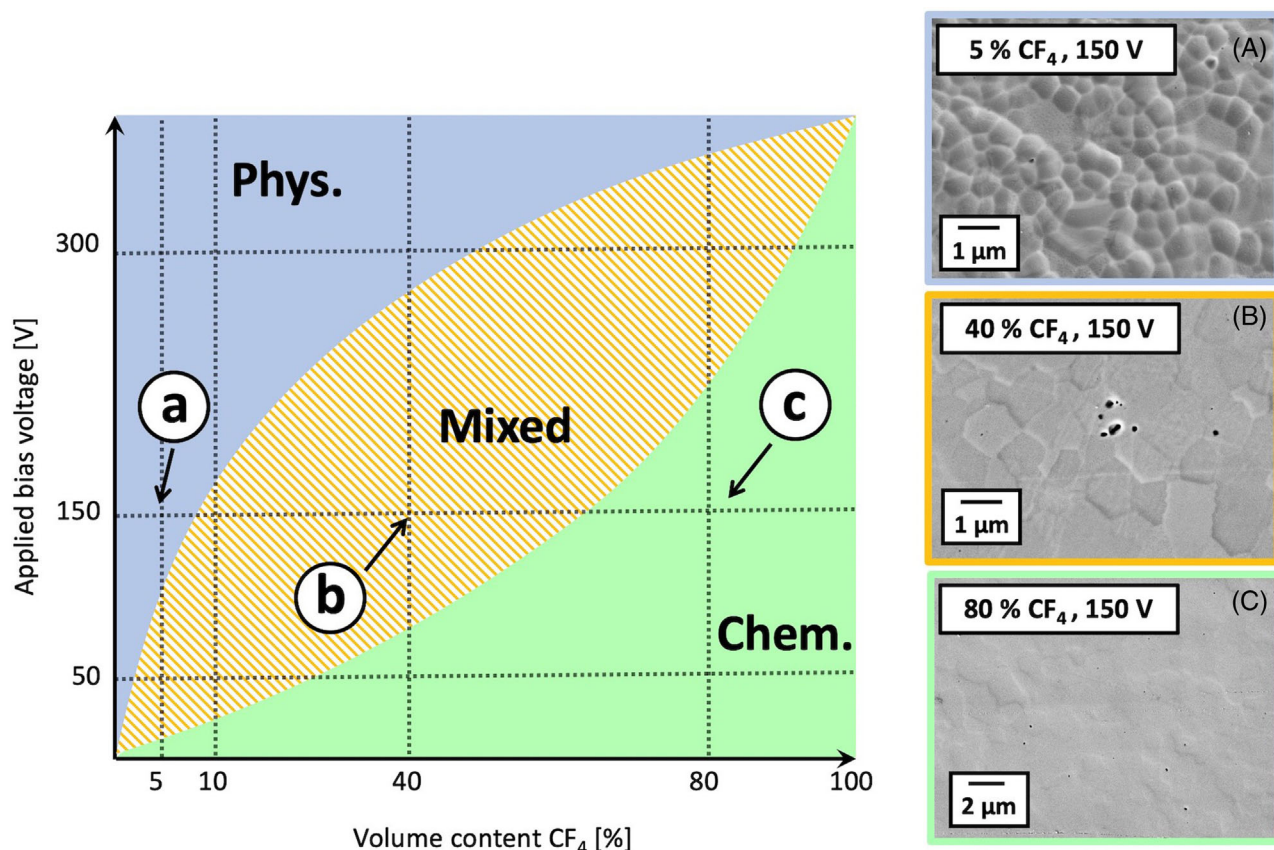
FIGURE 8 Schematic plasma processing map displaying the dominating erosion mechanisms for polycrystalline Y_2O_3 depending on the plasma parameters (P = physically driven, M = mixed, C = chemically driven erosion). (A–C) Additional SEM images of Y_2O_3 samples exposed to different plasma etching parameters are displayed to highlight the strong influence of the active mechanism on the erosion behavior and the formed surface morphology (Parameters as indicated)

mechanisms depending on the etching parameters and is expected to be helpful for predicting the lifespan under real plasma etching conditions.

The systematic variation of the bias voltage and plasma gas composition conducted during this study showed for the first time a distinct relationship between the plasma etching parameters and the specific kinds of erosion induced by fluorine-based plasmas on the example of polycrystalline Y_2O_3. The approach can be easily transferred to other ceramic materials that are in contact with reactive plasmas in the semiconductor industry. In general, our approach is the key of understanding the erosion behavior of novel plasma-faced materials in a systematic way and therefore allows to evaluate their potential with respect to their long-term use.

ORCID

Moritz Kindelmann https://orcid.org/0000-0001-9676-2090
Olivier Guillon https://orcid.org/0000-0003-4831-5725

REFERENCES

1. Iwasawa J, Nishimizu R, Tokita M, Kiyohara M, Uematsu K. Plasma-resistant dense yttrium oxide film prepared by aerosol deposition process. J Am Ceram Soc. 2007;90(8):2327–32. https://doi.org/10.1111/j.1551-2916.2007.01738.x
2. Miwa K, Takada N, Sasaki K. Fluorination mechanisms of Al2O3 and Y2O3 surfaces irradiated by high-density CF4/O2 and SF6/O2 plasmas. J Vac Sci Technol A Vacuum Surfaces Film. 2009;27(4):831–5. https://doi.org/10.1116/1.3112624
3. Ma T, List T, Donnelly VM. Y2O3 wall interactions in Cl2 etching and NF3 cleaning plasmas. J Vac Sci Technol A Vacuum Surfaces Film. 2017;35(3):31303.
4. Ma T, List T, Donnelly VM. Comparisons of NF3 plasma-cleaned Y2O3, YOF, and YF3 chamber coatings during silicon etching in Cl2 plasmas. J Vac Sci Technol A. 2018;36(3):31305. https://doi.org/10.1116/1.5026777
5. Yoshida H, Kodo M, Soga K, Yamamoto T. Doping effect on sinterability of polycrystalline yttria: From the viewpoint of cation

diffusivity. J Eur Ceram Soc. 2012;32(12):3103–14. https://doi.org/10.1016/j.jeurceramsoc.2012.04.010

6. Kim Y-C, Kim C-I. Etching mechanism of Y2O3 thin films in high density Cl2/Ar plasma. J Vac Sci Technol A Vacuum Surfaces Film. 2001;19(5):2676–9. https://doi.org/10.1116/1.1399316

7. Worhoff K, Bradley J, Ay F, Pollnau M. Reactive Ion Etching of Y2O3 films applying F-, Cl-and Cl/Br-based Inductively coupled plasmas. ECS Trans. 2006;3(11):117–24.

8. Jung J-H, Hahn B-D, Yoon W-H, Park DS, Choi JJ, Ryu J, et al. Halogen plasma erosion resistance of rare earth oxide films deposited on plasma sprayed alumina coating by aerosol deposition. J Eur Ceram Soc. 2012;32(10):2451–7.

9. Cao Y-C, Zhao L, Luo J, Wang K, Zhang BP, Yokota H, et al. Plasma etching behavior of Y2O3 ceramics: comparative study with Al2O3. Appl Surf Sci. 2016;366:304–9.

10. Lin T-K, Wang W-K, Huang S-Y, Tasi C-T, Wuu D-S. Comparison of erosion behavior and particle contamination in mass-production CF4/O2 plasma chambers using Y2O3 and YF3 protective coatings. Nanomaterials. 2017;7(7):183.

11. Oehrlein GS, Zhang Y, Vender D, Haverlag M. Fluorocarbon high-density plasmas. I. Fluorocarbon film deposition and etching using CF4 and CHF3. J Vac Sci Technol A Vacuum Surfaces Film. 1994;12(2):323–32.

12. Oehrlein GS, Zhang Y, Vender D, Joubert O. Fluorocarbon high-density plasmas. II. Silicon dioxide and silicon etching using CF4 and CHF3. J Vac Sci Technol A Vacuum Surfaces Film. 1994;12(2):333–44.

13. Kim D-M, Oh Y-S, Kim S, Kim H-T, Lim D-S, Lee S-M. The erosion behaviors of Y2O3 and YF3 coatings under fluorocarbon plasma. Thin Solid Films. 2011;519(20):6698–702.

14. Schaepkens M, Oehrlein GS. A review of SiO2 etching studies in inductively coupled fluorocarbon plasmas. J Electrochem Soc. 2001;148(3):C211.

15. Kim D-M, Kim K-B, Yoon S-Y, Oh Y-S, Kim H-T, Lee S-M. Effects of artificial pores and purity on the erosion behaviors of polycrystalline Al2O3 ceramics under fluorine plasma. J Ceram Soc Jpn. 2009;117(1368):863–7.

16. Ashizawa H, Yoshida K. Effect of the microstructures of yttria ceramics on their plasma corrosion behavior. Ceram Int. 2019;45(17):21162–7. https://doi.org/10.1016/j.ceramint.2019.07.093

17. Yoshida H, Morita K, Kim B-N, Hiraga K, Kodo M, Soga K, et al. Densification of nanocrystalline yttria by low temperature spark plasma sintering. J Am Ceram Soc. 2008;91(5):1707–10. https://doi.org/10.1111/j.1551-2916.2008.02337.x

18. Bram M, Laptev AM, Mishra TP, Nur K, Kindelmann M, Ihrig M, et al. Application of electric current-assisted sintering techniques for the processing of advanced materials. Adv Eng Mater. 2020;22(6):2000051. https://doi.org/10.1002/adem.202000051

19. Kindelmann M, Ran K, Rheinheimer W, Morita K, Mayer J, Bram M, et al. Segregation-controlled densification and grain growth in rare earth-doped Y2O3. J Am Ceram Soc. 2021;104(10):4946–59. https://doi.org/10.1111/jace.17907

20. Kindelmann M, Stamminger M, Schön N, Rasinski M, Eichel RA, Hausen F, et al. Erosion behavior of Y2O3 in fluorine-based

etching plasmas: Orientation dependency and reaction layer formation. J Am Ceram Soc. 2020;104(3):1465–74. https://doi.org/10.1111/jace.17556

21. Kindelmann M, Weber LM, Stamminger M, Buschhaus R, Wessel E, Bram M, et al. The role of fluorination during the physicochemical erosion of yttria in fluorine-based etching plasmas. J Am Ceram Soc. 2021;42(2):561–6.

22. Kim D-M, Lee S-MS-H, Alexander WB, Kim K-B, Oh Y-S, Lee S-MS-H. X-ray photoelectron spectroscopy study on the interaction of yttrium-aluminum oxide with fluorine-based plasma. J Am Ceram Soc. 2011;94(10):3455–9. https://doi.org/10.1111/j.1551-2916.2011.04589.x

23. Onderdelinden D. The influence of channeling on Cu single-crystal sputtering. Appl Phys Lett. 1966;8(8):189–90. https://doi.org/10.1063/1.1754548

24. Balden M, Bardamid AF, Belyaeva AI, Slatin KA, Davis JW, Haasz AA, et al. Surface roughening and grain orientation dependence of the erosion of polycrystalline stainless steel by hydrogen irradiation. J Nucl Mater. 2004;329–333:1515–9. https://doi.org/10.1016/j.jnucmat.2004.04.240

25. Voitsenya VS, Balden M, Belyaeva AI, Alimov VKh, Tyburska-Püschel B, Galuza AA, et al. Effect of sputtering on self-damaged recrystallized W mirror specimens. J Nucl Mater. 2013;434(1):375–81. https://doi.org/10.1016/j.jnucmat.2012.12.007

26. Ling L, Hua X, Zheng L, Oehrlein GS, Hudson EA, Jiang P. Studies of fluorocarbon film deposition and its correlation with etched trench sidewall angle by employing a gap structure using C4F8/Ar and CF4/H2 based capacitively coupled plasmas. J Vac Sci Technol B Microelectron Nanom Struct Process Meas Phenom. 2008;26(1):11–22. https://doi.org/10.1116/1.2817627

27. Kim M, Efremov A, Hong M, et al. Effect of gas mixing ratio on etch behavior of Y2O3 thin films in Cl2/Ar and BCl3/Ar inductively coupled plasmas. Jpn J Appl Phys. 2010;49(8S1):08JB04.

28. Kwon K, Kim Y, Efremov A, Kim K. On the dry etch mechanisms of Y2O3, SiO2, and Si3N4 in a Cl2/BCl3 inductively coupled plasma. J Korean Phys Soc. 2011;58(3):467–71.

SUPPORTING INFORMATION

Additional supporting information may be found in the online version of the article at the publisher's website.